Development of Calculation Technique for FEM Thermal Simulation Using Virtual Fluid Elements

IKUO TANABE
School of Engineering
Sanjo City University
5002-5 Kamisugoro, Sanjo, Niigata
JAPAN

HIROMI ISOBE
Department of Mechanical Engineering
Nagaoka University of Technology
1603-1 Kamitomioka, Nagaoka, Niigata
JAPAN

Abstract: - In recent years, CAE (Computer-aided engineering) using FEM (Finite element method) simulations were generally used in the design field. FEM simulations were classified as static implicit and explicit dynamics methods. Particularly FEM simulations using the static implicit method were very generally and usefully used in the industrial world. The static implicit method FEM consists of static, buckling, thermal, vibration analyses, and so on. This FEM thermal analysis can't calculate the phenomena of heat transfer and internal forced cooling in some enclosures of a machine tool. On the other hand, when the temperature distributions in a structure such as that are calculated, FVM fluid simulation was used for that. However, this simulation can't exactly calculate a complex structure in a machine tool, needs very long calculation times and the calculation accuracy is very poor. Therefore, in this research, the calculation technique regarding FEM thermal simulation using 4 virtual fluid elements was developed and evaluated for the phenomena of heat build-up and internal forced cooling in some enclosures of a machine tool. The algorithms and the calculation models regarding 4 virtual fluid elements were developed, then the proposed method was evaluated in the experiment. It is concluded from the results that; (1) the 4 virtual fluid elements were developed for FEM thermal simulation instead of FVM fluid simulation, (2) FEM thermal simulation with the developed 4 virtual fluid elements has high calculation accuracy and a short calculation time, (3) the proposed method was very effective in the design.

Key-Words: - FEM thermal simulation, Virtual fluid elements, FVM fluid simulation, Machine tool design, CAE, Virtual technique

Received: May 22, 2022. Revised: January 6, 2023. Accepted: February 17, 2022. Published: March 20, 2023.

1 Introduction

Recently, in the design phase, it is often necessary to perform fluid analysis of industrial products using FVM fluid simulation, [1]. Particularly, in the field of thermal design, [2], [3], [4], [5], [6], it's a very important technology. However, FEM thermal simulation is more prevalent than FVM technology in the industrial world, [7]. In addition, FEM thermal simulation is easier to operate than FVM fluid simulation and can be used more quickly. However, FEM thermal analysis can't calculate the phenomena of heat build-up and internal forced cooling in some enclosures of a machine tool. On the other hand, when the temperature distributions in a structure such as that are calculated, FVM fluid simulation was used for that. However, this simulation can't exactly calculate a complex structure in a machine tool, needs very long calculation times and the calculation accuracy is very poor.

In this study, 4 virtual fluid elements (hereinafter referred to as "virtual fluid elements") were developed and evaluated in order to substitute FEM thermal simulation for FVM fluid simulation. Then the algorithm for these virtual fluid elements was constructed and evaluated its overall industrial effectiveness by experimentally evaluating its computational time and error.

2 Explanation Regarding 4 Virtual Elements for FEM Thermal Simulation

2.1 Outline for 4 Virtual Fluid Elements

Figure 1 shows the four virtual fluid elements of the structure to be analyzed. This represents the behavior of the flowing medium in the structure. It consists of four elements; I: Simulated element for inflow, II: Simulated element for outflow, III: Simulated element for the boundary layer, and IV: Simulated element for convection.

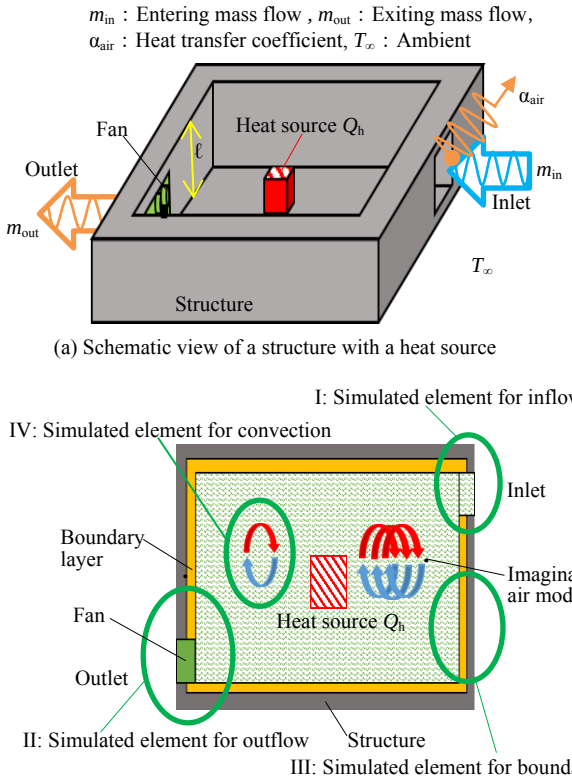

(a) Schematic view of a structure with a heat source

(b) Schematic view of analysis object for FEM thermal simulation instead of FVM fluid simulation

Figure 1: Analysis object for FEM thermal simulation instead of FVM fluid simulation. Four virtual elements *I*, *II*, *III* and *IV* were used for the FEM thermal simulation.

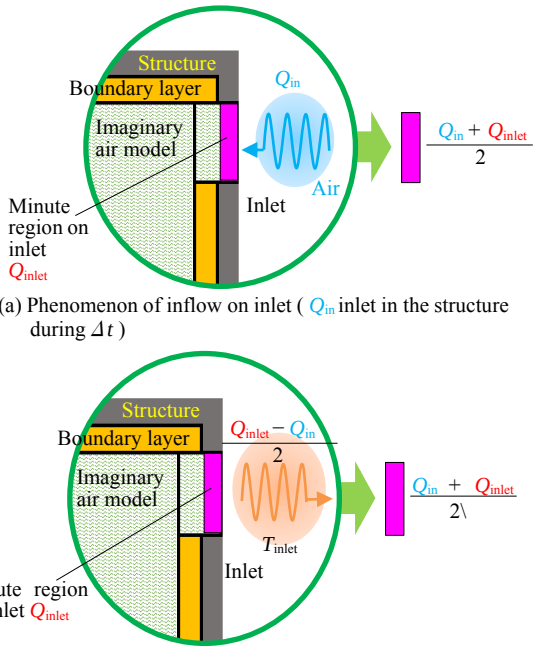

(a) Phenomenon of inflow on inlet (Q_{in} inlet in the structure during Δt)

(b) Heat transfer of I: Simulated element for inflow (($Q_{inlet}-Q_{in}$) / 2 outlet from the structure during Δt

Figure 2: Explanation of I: Simulated element for inflow. Heat capacity of the inflow was supposed by heat transfer.

$$(Q_{inlet}-Q_{in})/2$$
$$= (\rho_{air}A_{in}V_{in}\Delta t\, c_{air}T_{inlet}-\rho_{air}A_{in}V_{in}\Delta t\, c_{air}T_\infty)/2$$
$$= \alpha_{inlet}A_{in}(T_{inlet}-T_\infty)\Delta t \quad (1)$$
$$\alpha_{inlet} = \rho_{air}V_{in}c_{air}/2 \quad (2)$$

2.2 I: Simulated Element for Inflow

As shown in Figure 2(a), at time $t = 0$ [s], the flowing medium in the micro-region near the structure inlet has a heat quantity Q_{inlet}. Then, during Δt [s], a flowing medium with a heat quantity Q_{in} smaller than Q_{inlet} flows into this micro-region, and the air in the micro-region is cooled. As a result, the heat content of the air in a small region is $(Q_{in}+Q_{inlet})/2$.

Next, in the case of the I: Simulated element for inflow, as shown in Figure 2(b), there is no flowing medium from the outside during the period from time $t = 0$ [s] to Δt [s] (no state shown in Figure 2(a)), during which heat is dissipated on the inlet surface of the structure by the heat transfer with the outside $(Q_{inlet} - Q_{in})/2$. The heat content of the flowing medium in the micro-region near the inlet of the structure during Δt s becomes $(Q_{in} + Q_{inlet})/2$, which is thermally equivalent to the state shown in Figure 2(a).

This equivalence is shown in Equation (1).

where ρ_{air} is density [kg/m^3], A_{in} is the cross-sectional area of the inlet of the structure [m^2], V_{in} is the velocity of the inflowing medium [m/s], c_{air} is the specific heat of the flowing medium [J/kg-K], T_∞ is outside flowing medium temperature [K], T_{inlet} is structure inlet temperature [K] and α_{inlet} is heat transfer coefficient with the outside on the αinlet structure inlet surface [W/m^2-K]. By hypothetically making the structure inlet have a heat transfer coefficient αinlet is possible to simulate the entry of a flowing medium with the heat quantity Q_{in} from the structure inlet.

2.3 II: Simulated Element for Outflow

As shown in Figure 3, at the outlet of the structure, a fluidized medium with a heat quantity Q_{out} [J] is evacuated in Δt [s] by forced evacuation by a fan. In the case of the II: simulated element for outflow, the actual forced exhaust is simulated by dissipating the heat quantity Q_{out} [J] in Δt [s] by heat transfer with the outside of the structure outlet. This equivalence is

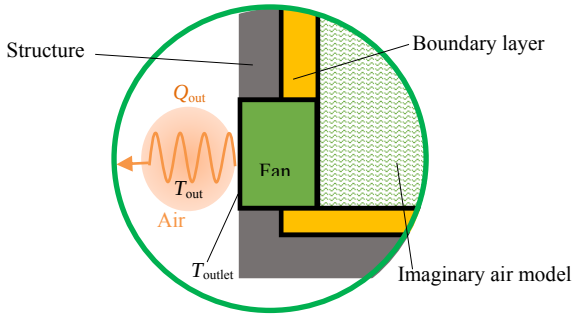

Figure 3: Explanation of II: Simulated element for outflow (Q_{out} outlet in the structure during Δt). Heat capacity of the outflow was supposed by heat transfer.

shown in Equations (3) and (4).

$$Q_{out} = \rho_{air} A_{out} V_{out} \Delta t \, c_{air} T_{out}$$
$$= \alpha_{outlet} (T_{out} - T_{\infty}) A_{out} \Delta t \quad (3)$$
$$\alpha_{outlet} = \rho_{air} V_{out} c_{air} / (1 - T_{\infty} / T_{outlet}) \quad (4)$$

where A_{out} is the cross-sectional area of the exit surface of the structure [m^2], V_{out} is the velocity of the outflowing medium [m/s], and T_{out} is the average temperature of the outflowing medium [K]. α outlet is the heat transfer coefficient on the exit surface of the structure[W/m^2-K]. Where the medium volume flowing out from the structure in Δt [s] ($A_{out}V_{out}\Delta t = A_{in}V_{in}\Delta t$) is small, the average temperature T_{out} of the outflowed medium is taken to be equivalent to the temperature T_{outlet} on the exit surface of the structure ($T_{out} = T_{outlet}$). By using the heat transfer coefficient α_{outlet} as a boundary condition on the structure outlet in FEM thermal simulation, it is possible to simulate the forced exhaust from the structure.

2.4 III: Simulated Element for Boundary Layer

As shown in Figure 4, the heat quantity Q_b is transferred by heat transfer between the inner wall of the structure and the flowing medium in the structure in Δt [s]. In this case, the amount of heat transfer at the wall surface of the structure by the heat transfer is referred to as Q_b [J]. In the case of the III: simulated element for the boundary layer, the thermal conductivity λ_b [W/m-K] is set to simulate the heat transfer. The equivalent states are shown in Equation (5).

$$Q_b = \alpha_w (T_{b1} - T_{b2}) A_w \Delta t = (\lambda_b / l_b) (T_{b1} - T_{b2}) A_w \Delta t,$$
$$\lambda_b = \alpha_w l_b \quad (5)$$

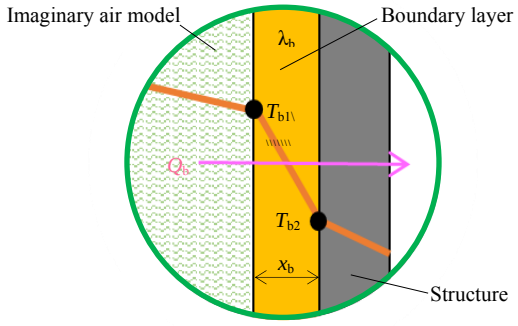

Figure 4: Explanation of III: Simulated element for boundary layer (Q_h transfer to the structure during Δt). Heat transfer of the boundary layer was supposed by heat conduction.

Where, αw is the heat transfer coefficient of the inner wall of the structure [W/m^2-K], Tb1 is the temperature of the boundary layer in contact with the III: simulated element for boundary layer [K], T_{b2} is the temperature of the inner wall of the structure in contact with the boundary layer [K], A_w is the surface area of the inner wall of the structure [m^2], λ_b is the thermal conductivity of the boundary layer [W/m-K] and l_b is the thickness of the boundary layer [m]. Although this l_b can be any value, we henceforth fix l_b = 0.003 m in this research because there are enough virtual fluid elements in the structure and the FEM mesh model is not too fine.

2.5 IV: Simulated Element for Convection

The energy balance of the flow medium in the structure is considered by replacing it with the elements shown in Figure 5. Considering the energy balance, [8], the following assumptions are made. a: The velocity and temperature fields are steady, and the airflow is laminar. b: The physical properties (density, viscosity, thermal conductivity, and specific heat at constant pressure) are constant. c: Ignoring heat generation in viscous work. As the thermal conductivity of the IV: simulated element for convection is presented in Figure 5, the pseudo-thermal conductivity λ_{cx} (heat transfer coefficient that simulates the convection phenomenon) is defined. The heat quantity Q_{cx} [J] moving through the elements in Δt seconds is given by Equation (6). The heat transfer $Q_{cx'}$ [J/s] per unit time due to the heat transfer caused by the temperature difference between the two ends of the elements in Figure 5 is given by Equation (7). In the x-axis direction, the difference between the energy exerted by convection from the right side of the microelement and the energy inflowed by convection from the left side of the microelement is given by Equation (8). Since the sum of the heat transferred by heat conduction in Equation (7) and the

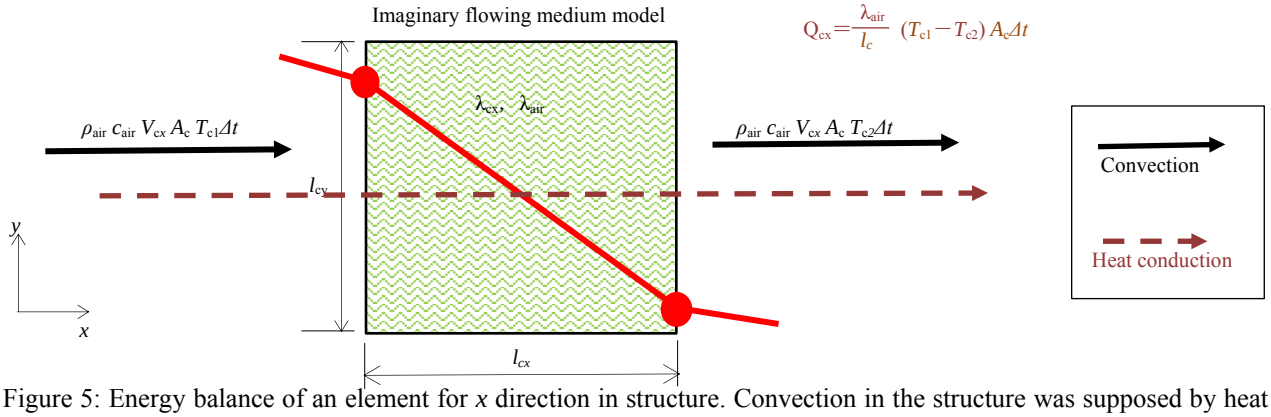

Figure 5: Energy balance of an element for *x* direction in structure. Convection in the structure was supposed by heat conduction.

energy transferred by convection in Equation (8) is the heat of Equation (6), Equation (9) is obtained. To organize this Equation (9), the pseudo-thermal conductivity λ_{cx} is shown in the equation from Equation (10), the pseudo-thermal conductivity of a virtual fluid element to simulate convection can be obtained; we have proposed the pseudo-thermal conductivity λ_{cx} in the x-direction, but the pseudo-thermal conductivities λ_{cy} and λ_{cz} in the y-direction and z-direction can also be obtained by the same equation.

$$Q_{cx} = (\lambda_{cx} / l_{cx})(T_{c1} - T_{c2})\, A_c\, \Delta t \quad (6)$$

$$Q_{cx}' = (\lambda_{air} / l_c)(T_{c1} - T_{c2})\, A_c\, \Delta t \quad (7)$$

$$\rho_{air}\, c_{air}\, V_{cx}\, A_c\, T_{c1}\, \Delta t - \rho_{air}\, c_{air}\, V_{cx}\, A_c\, T_{c2}\, \Delta t = \rho_{air}\, c_{air}\, V_{cx}\, A_c\, (T_{c1} - T_{c2})\, \Delta t \quad (8)$$

$$\rho_{air}\, c_{air}\, V_{cx}\, A_c\, (T_{c1} - T_{c2})\, \Delta t + (\lambda_{air} / l_c)(T_{c1} - T_{c2}) A_c\, \Delta t = (\lambda_{cx} / l_{cx})(T_{c1} - T_{c2})\, A_c\, \Delta t \quad (9)$$

$$\lambda_{cx} = \lambda_{air} + \rho_{air}\, c_{air}\, V_{cx}\, l_{cx} \quad (10)$$

Where λ_{cx} is the pseudo-thermal conductivity of the element in the x-direction [W/m-K], l_{cx} is the length of the element in the x-direction [m], Tc1 is the temperature of the left end of the element [K], Tc2 is the temperature of the right end of the element [K], A_c is the cross-sectional area of the yz plane of the element [m^2], λ_{air} is pseudo-thermal conductivity of the flow medium in the x-direction [W/m-K], V_{cx} is the average velocity of air in the x-direction [m/s].

3 Evaluation Experiment Regarding 4 Virtual Fluid Element Models

3.1 Experimental Models and Experimental Conditions for Evaluation

Experiments were conducted on three models to evaluate the effectiveness of the proposed 4 virtual fluid elements. First, a complex model for the evaluation experiment is shown in Figure 6, with one fan, two shielding walls, and ceramic heaters in two locations. The fluid medium is air. For the simple model, two shielding walls and one heater were removed from the complex model. As shown in Figure 6(b), thermocouples were installed inside the enclosure and around the periphery of the enclosure in all experiments (16 points for simple models and 26 points for complex models) and measured until the temperature of the air or cutting fluid reached steady state, respectively. In the forced cooling with cooling oil for the complex structural model shown in Figure 7 (for the third model), the previous complex enclosure was appropriated and cooling oil was used instead of air. The intake and exhaust ports of the enclosure in the complex model were modified to a nipple structure so that the coolant oil can be easily supplied, and the enclosure was erected so that the inlet is downward and the outlet is upward. As shown in Table 1, two types of exhaust velocity, two types of the heating value of the heater, and two types of cooling oil inflow were used as the parameters of the experiment. The room temperature was 20±1°C.

3.2 Calculation Models and Its Analysis Condition for Evaluation

The three experiments in the previous section were calculated using SolidWorks 2017. Figure 8 shows the computational models of FEM thermal simulation and FVM fluid simulation for the complex model, respectively, as representatives of each computational model. The FVM fluid simulation is performed using Flow simulation, a fluid analysis software on SolidWorks 2017, and the discretization method is the finite volume method. For comparison, the number of nodes in the FEM thermal simulation model and the number of elements in the FVM fluid simulation model are almost the same. Table 2 and

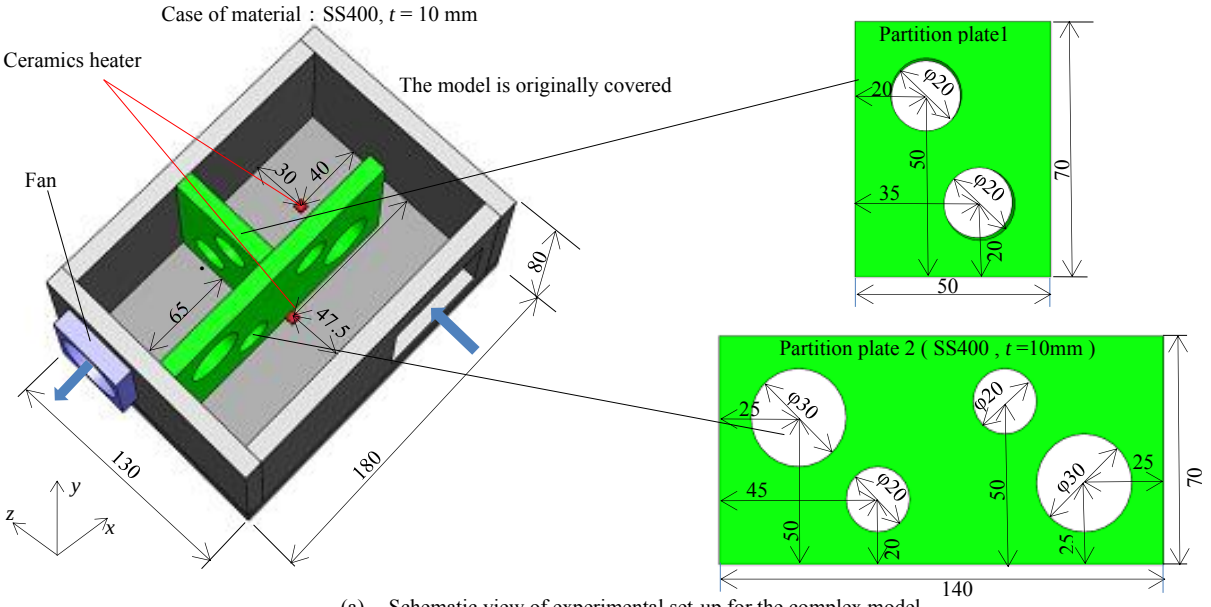

(a) Schematic view of experimental set-up for the complex model

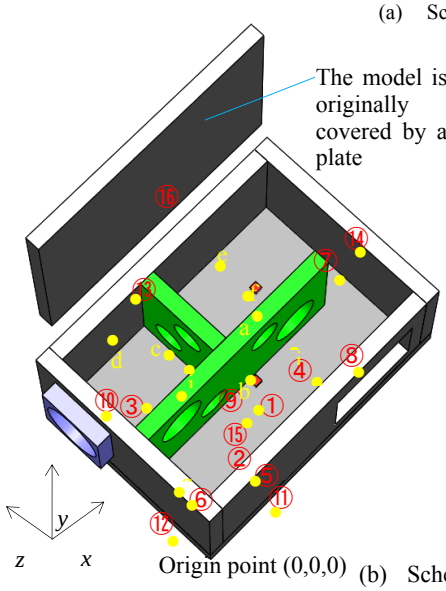

(b) Schematic view of experimental set-up with several thermocouples

Point	Coordinate	Point	Coordinate	Point	Coordinate
①	(90,11.75,57.5)	⑪	(45,45,0)	e	(130,45,120)
②	(45,10,40)	⑫	(0,45,35)	f	(140,45,100)
③	(45,10,90)	⑬	(90,45,130)	g	(70,45,65)
④	(115,10,40)	⑭	(130,45,65)	h	(15,45,55)
⑤	(45,45,10)	⑮	(90,0,65)	i	(125,35,65)
⑥	(10,45,35)	⑯	(65,90,65)	j	(80,60,80)
⑦	(170,45,65)	a	(130,11.75,100)	Thermocouples installed in the same place as only ①～⑯ in the case simple model.	
⑧	(155,15,20)	b	(90,45,50)		
⑨	(90,45,57.5)	c	(75,45,85)		
⑩	(20,50,95)	d	(50,45,120)		

Figure 6: Schematic view of experimental set-up for evaluation of the proposed virtual elements using the complex model. In case of the simple model, the green two parts with several holes were removed. In case of the complex model with forced cooling oil, the inlet and the outlet of the model were remade using two nipples.

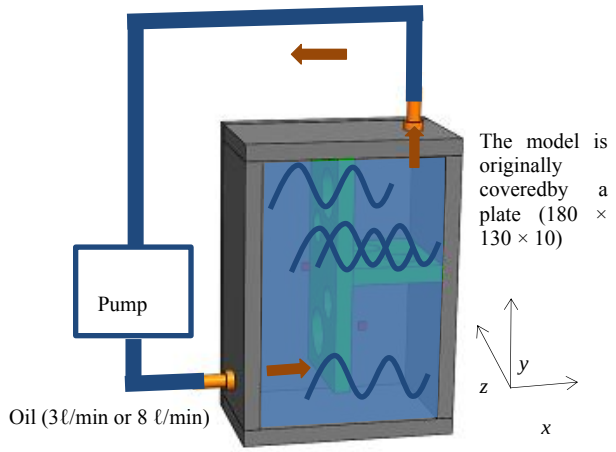

Figure 7: Schematic view of experimental set-up using the complex model with forced cooling oil (See Table 1 for the experimental conditions).

Table 1. Experimental conditions and equipment for evaluation of proposed

Air outlet velocity m/s (Voltage applied to the fan V)	0.5 , 1.0 (3.5 , 5)
Input power to ceramics heater W	5 , 12
Oil inflow rate ℓ/min (Oil inlet velocity m/s)	3 , 8 (2.6 , 6.9)
Temperature of inflowing air and oil ℃(Oil temperature is controlled by a thermostat)	20
Ambient temperature ℃	20
Thermocouple	Type T
Distance between fan and anemometer mm	100
Anemometer (KANOMAX)	6151
Data logger (YOKOGAWA)	MV-230
Slidac (MATSUNAGA)	SD-1310
Power supply (TAKASAGO)	GPV 035-20
Pump (KYOWA)	KYC-300-1
Flowmeter (HORIBA)	LW5-TTN

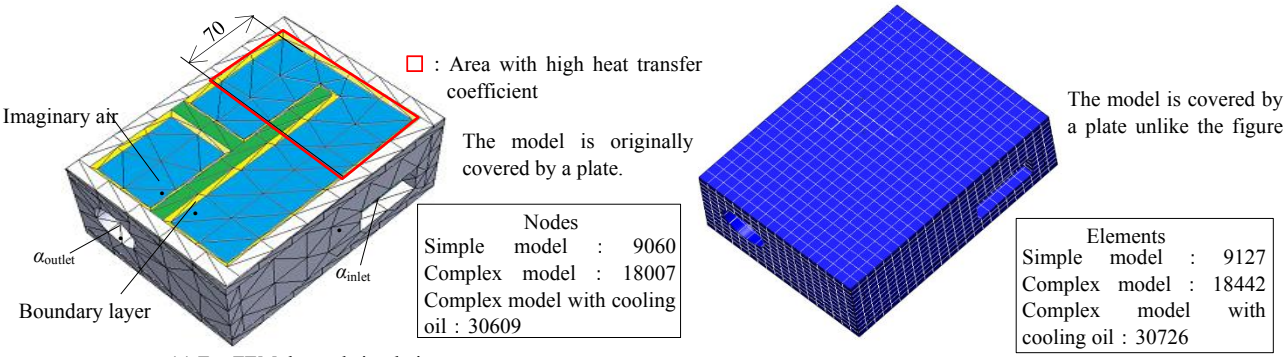

(a) For FEM thermal simulation (b) For FVM fluid simulation

Figure 8: Schematic views of calculation models of complex model

Table 2: Calculation conditions of FVM fluid simulation.

Condition of fluid simulation (ρ : Density, c : Specific heat, λ : Thermal conductivity, μ : Viscosity)		
Wall condition	α_{air} = 5 [W/m^2・K]	
Initial solid temperature	20 ℃	
Input power to ceramics heater	5 W , 12 W	
Boundary condition	Simple model and complex model	Condition of inlet : Static pressure Outlet velocity : 0.5 m/s , 1.0 m/s
	Complex model with cooling oil	Oil inflow rate : 3 ℓ/min (2.6m/s) , 8 ℓ/min(6.9m/s) Condition of outlet : Static pressure Oil temperature entered
Convergence condition of steady simulation	End of calculation of temperature and heat transfer coefficient or all possible values	
Unsteady simulation	All physical time : 3600 s , Time step : 10 s	

Table 3: Calculation conditions of FEM thermal simulation and boundary conditions for proposed imaginary air element; four virtual elements in Figure 1 were supposed.

Condition of thermal simulation (ρ : Density, c : Specific heat, λ : Thermal conductivity, μ : Viscosity)			
Simulation solver		Intel direct sparse	
Unsteady simulation		All physical time : 3600 s , Time step : 10 s	
Wall condition		α_{air} = 5 [W/m^2・K]	
Initial solid temperature Temperature of inlet		20 ℃, Oil :Oil temperature entered	
Input power to ceramics heater P		5 W , 12 W	
Boundary condition		Inlet	α_{inlet}
		Outlet	α_{outlet}
Physical properties of parts	Imaginary air element	Simple model and complex model	ρ : 1.293 kg/m^3 , c : 1006 J/(Kg・K) , λ : λ_c
		Complex model with cooling oil	ρ : 893 kg/m^3 , c : 2878 J/(Kg・K) , λ : λ_c
	Boundary layer element	Simple model and complex model	ρ : 1.293 kg/m^3 , c : 1006 J/(Kg・K) , λ : λ_b
		Complex model with cooling oil	ρ : 893 kg/m^3 , c : 2878 J/(Kg・K) , λ : λ_b

Boundary condition for proposed imaginary air element						
FEM model	Velocity of liquid V m/s	α_{inlet} (Equation 4) W/m^2・K	α_{outlet} (Equation 7) W/m^2・K	λ_b (Equation 10) W/m・K	V_c (Equation 9) (V_x , V_y , V_z) m/s	λ_c (Equation 9) W/m・K
Simple model	Outlet velocity : 0.5	217	30 ℃:18400,40 ℃:9510, 50 ℃:6500,60 ℃:5050	0.00480 0.0129	(0.0698, 0.0305, 0.0480) (0.521, 0.228, 0.358)	(13.6, 2.61, 6.41) (101, 19.4, 47.8)
	Outlet velocity : 1.0	434	30 ℃:36900,40 ℃:19000, 50 ℃:13100,60 ℃:10100	0.00679 0.0199	(0.140, 0.0611, 0.0960) (1.04, 0.456, 0.717)	(27.1, 5.20, 12.8) (202, 38.7, 95.5)
Complex model	Outlet velocity : 0.5	217	30 ℃:18400, 40 ℃:9510, 50 ℃:6500,60 ℃:5050	0.00480 0.0129	(0.0698, 0.0305, 0.0480) (0.521, 0.228, 0.358)	(13.6, 2.61, 6.41) (101, 19.4, 47.8)
	Outlet velocity : 1.0	434	30 ℃:36900,40 ℃:19000, 50 ℃:13100, 60 ℃:10100	0.00679 0.0199	(0.140 , 0.0611 , 0.0960) (1.04, 0.456, 0.717)	(27.1, 5.20, 12.8) (202, 38.7, 95.5)
Complex model with cooling oil	Inlet velocity : 2.6	3.1×10^6	30 ℃:1.92×10^7,40 ℃:9.93×10^7, 50 ℃:6.83×10^7, 60 ℃:5.27×10^7	0.0532 4.06	(0.00284, 0.00649, 0.00446) (2.55, 5.82, 6.48)	(496, 2590, 1230) (4.45×10^5, 2.32×10^6, 1.78×10^6)
	Inlet velocity : 6.9	8.4×10^6	30 ℃:5.11×10^8,40 ℃:1.90×10^8, 50 ℃:1.31×10^8, 60 ℃:1.01×10^8	0.0869 7.31	(0.00758, 0.0173, 0.0119) (6.79, 15.5, 10.7)	(1320, 6910, 3270) (1.19×10^6, 6.20×10^6, 2.93×10^6)

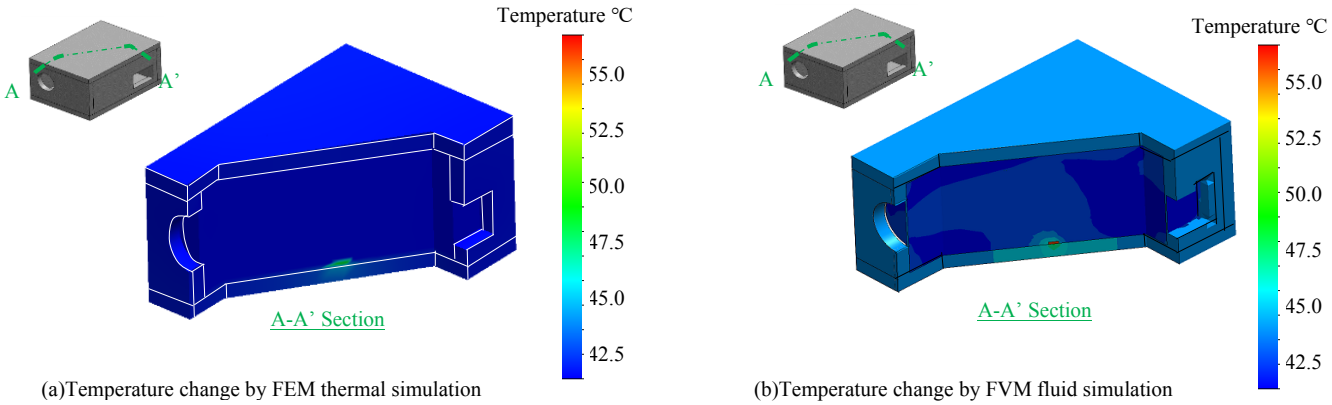

(a)Temperature change by FEM thermal simulation (b)Temperature change by FVM fluid simulation

Figure 9: Calculation results for temperature change using the simple model with 5 W power and 0.5 m/s velocity. In case of the FVM fluid simulation, there are the disproportionate temperature distribution because of the real flow influences.

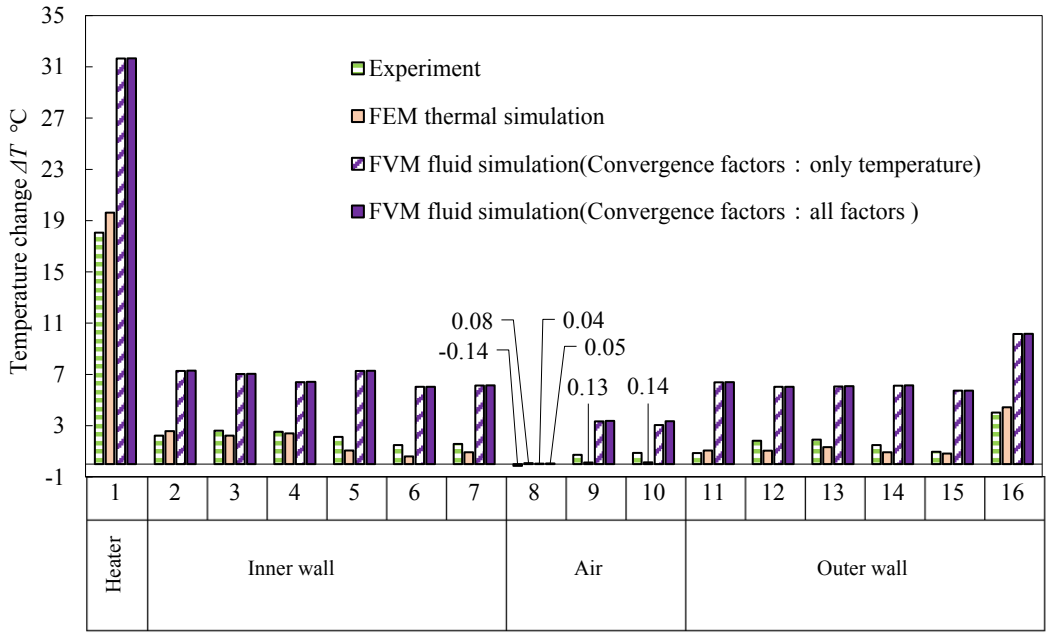

Figure 10: Results for temperature change distribution using the simple model with 5 W power and 0.5 m/s velocity. Calculated results without the adjustment of the boundary conditions using FEM thermal simulation unexpectedly were suit to the experimental results.

Table 3 shows the analytical conditions of the FVM fluid simulation and FEM thermal simulation, respectively.

3.3 Comparison of Experimental and Calculated Results

Figure 9(a) and Figure 9(b) show examples of the calculated results (temperature distribution) of FEM thermal and FVM fluid simulations, respectively. A simple model is used to show the distribution of steady-state temperature rise values when 5 W of power is applied to a single ceramic heater and the air is expelled from the outlet at a rate of 0.5 m/s.

Figure 10 shows the temperature distribution in Figure 9. The experimental values corresponding to the thermocouple positions and the calculated results of FEM thermal simulation, FVM fluid simulation (convergence condition for temperature only), and FVM fluid simulation (convergence condition for all possible values) are shown, respectively. These experiments and three types of analyses resulted in a total of 24 pairs of results (= 3 × 4 × 2), with three models, four combinations of conditions, and two types of steady-state and non-steady-state analyses; Figure 9 and Figure 10 are examples.

Figure 11 shows the results of FEM thermal simulation and FVM fluid simulation using the virtual fluid element proposed in this paper, comparing the analysis time and the error based on the experimental temperature distribution in the enclosure, respectively. Here, we evaluate three types of analysis results based on the results of the previous

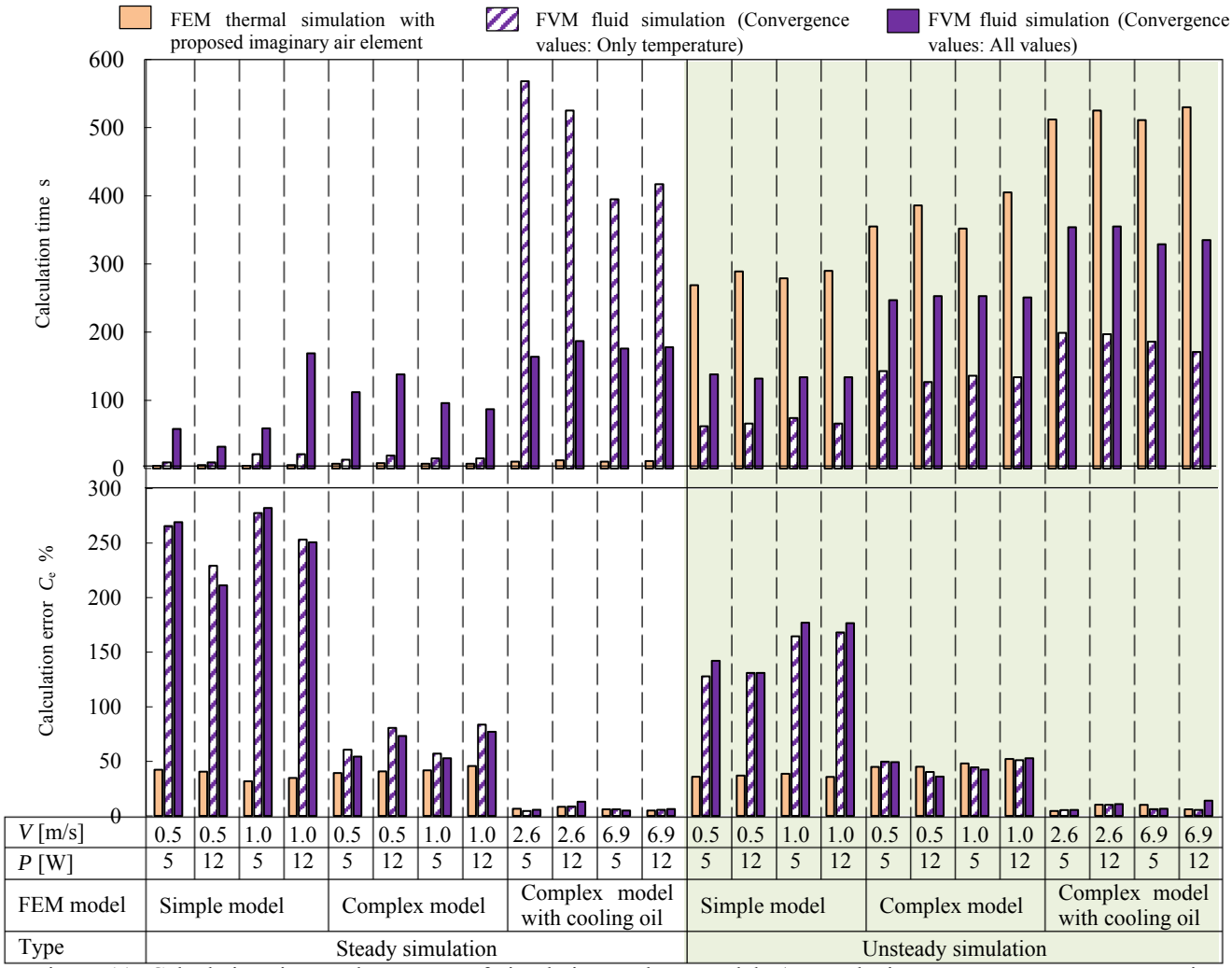

Figure 11: Calculation time and accuracy of simulation at three models (V : Velocity, P : Input power to ceramics heater). Calculation times for the FEM thermal unsteady simulation were very longer than that of the FVM fluid simulation. And calculated results without the adjustment of the boundary conditions using FEM thermal simulation unexpectedly were nearly to the experimental results. Therefore, the FEM thermal simulation using the proposed 4 virtual elements was used for a design instead of FVM fluid simulation.

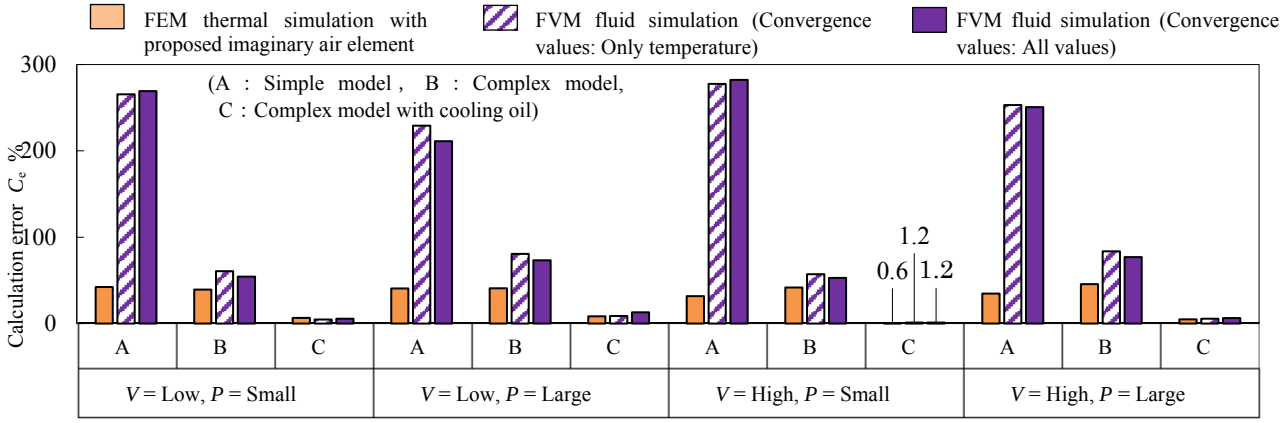

Figure 12: Accuracy of analysis at three models focusing on the conditions of radiation and flow (Please see Table 4 and Figure11 regarding “Low”, “High”, “Small” and “Large” for V and P respectively). When the air velocity was changed from 0.5 m/s to 1.0 m/s, the oil velocity was changed from 2.6 m/s to 6.9 m/s and the input power to the ceramics heaters were changed from 5 W to 12 W, the calculated results without the adjustment of the boundary conditions using FEM thermal simulation unexpectedly were nearly to the experimental results. The FEM thermal simulation using the proposed 4 virtual elements was used for a design instead of FVM fluid simulation.

24 pairs of experiments. Both steady-state and unsteady-state conditions are summarized. In the non-steady state, the results are calculated in 10-second steps over the 1 hour from the start. The calculation error was calculated by Equation (11), using 16 points for the simple model and 26 points for the complex model, both inside and outside the enclosure.

$$C_e = \left[\sum_{n=1}^{16 \text{ or } 26} \left|(T_{c\text{-}n} - T_{e\text{-}n})/T_{e\text{-}n}\right|\right] \div (16 \text{ or } 26) \times 100 \quad (11)$$

where C_e is the calculation error [%], $T_{e\text{-}n}$ is the experimental temperature rise at n points in the enclosure [°C], and $T_{c\text{-}n}$ is the calculated temperature rise at n points in the enclosure [°C].

For steady-state conditions, regarding calculation time, the FEM thermal simulation using the proposed virtual fluid element was shorter than the FVM fluid simulation by about 4/9 to 1/285. The fluid analysis of a complex model using a cutting oil agent did not converge after more than 24 hours of calculation, so the number of elements was reduced from 30726 to 7667, resulting in convergence. The calculation errors for the FEM thermal simulation with virtual fluid elements are 7/8 to 1/9 of one of the FVM fluid simulations. The reason why the steady-state analysis takes longer for the FVM fluid simulation than for the FEM thermal simulation is thought to be due to the difference in the discretization of the analysis. For the unsteady state, regarding calculation time, the FEM thermal simulation with the proposed virtual fluid element takes about 2.1 to 3.1 times longer than the FVM fluid simulation. This may be due to the time required to calculate the convergence of the four virtual fluid elements. The computational errors of FEM thermal simulations with virtual fluid elements are 6/7 to 1/9 of one of the FVM fluid simulations. It can be concluded that the proposed FEM thermal simulation using virtual fluid elements can be calculated accurately for both steady-state and unsteady-state analyses, and especially for steady-state analyses, the analysis time is shorter than that of FVM fluid simulation. In general, a general evaluation is often made by steady-state thermal analysis, as exemplified by the design of a heat sink inside a personal computer. Therefore, the proposed FEM thermal simulation with virtual fluid elements is considered to be very effective in terms of both analysis time and calculation accuracy.

Figure 12 shows a comparison of the calculated steady-state temperature rise values in Figure 11, adjusted for the high and low inflow and outflow velocities of the cooling medium and the large and small input power of the ceramic heater; the calculated results showed similar trends for three types of experiments (A; simple model + air, B; complex model + air, and C; complex model + cutting oil) without being affected by the high and low inflow and outflow velocities of the cooling medium or the large and small input power of the ceramic heater. It can be seen that the FEM thermal simulation using virtual fluid elements is more accurate than the FVM fluid simulation, about 7/8 to 1/9. In addition, the FEM thermal simulation proposed in this paper can accurately reflect the effect of the temperature change of the enclosure due to the difference in the characteristics of laminar-turbulent flow due to the increase in the heating value of the heat source and the change in the velocity of the medium.

4 Considerations for Applying the Proposed Method to Actual Machine Tools

In this chapter, the four proposed virtual fluid elements will be used in the future to study the phenomenon of heat buildup in the actual machine tool structure and the FEM thermal simulation of forced air intake and exhaust into and out of the machine structure.

As shown in Table 4, a machine tool consists of a main structure such as a spindle head and bed, as well as thermal-volumetric spaces (TVS) such as safety enclosures and piping. Heat sources in machine tools include spindle bearings, ball screws and ball nuts, linear guides, and motors, as well as heat generated by cutting tools and workpieces, accumulated chips, and cutting fluid. These heat sources mainly conduct heat within the machine structure, causing thermal deformation and loss of machining accuracy. Apart from that, these heat sources also transfer heat to the fluid (mainly air) in the enclosure or thermal volume space TVS, causing the fluid to rise in temperature, which again transfers heat to the machine structure, resulting in complex thermal deformation and reduced machining accuracy. This also causes heat buildup, which is counteracted by forced air intake and exhaust into the machine structure.

In this research, the four proposed virtual fluid elements were evaluated using simple models. When applying the elements to actual machine tools with complex specifications (shape, size, material, number of machine elements, etc.), the FEM models can be easily created using current CAD software, and complex thermal conditions can be easily set. Therefore, it is easy to set up I: Simulated element for

Table 4: Considerations for applying the proposed four virtual models to real machine tools.

Structures containing fluids in machine tools.	Sources of heat generated during machine tool operation	Thermal effects of the sources
・Main structures as a machine tool element (Head stock, Bed and so on), and complex ribbed structures in main structures ・Accessories (NC controller, oil tank and so on) ・Enclosures for safety ・Thermal-Volimetric Spaces (Other spaces such as plumbing)	・Spindle bearings, ball screws and ball nuts, linear guides and motors for operation ・Workpieces, Tools and Chips for heat generated during cutting ・Cutting fluids for forced cooling (as a heat source here)	・Heat conduction to machine structure → Thermal deformation → Reduced accuracy ・Heating the fluid in the enclosures and the thermal-volimetric spaces → The deformation for the fluid→ Reduced accuracy

inflow and II: Simulated element for outflow out of the four proposed virtual fluid elements. In addition, as mentioned above, III: Simulated element for the boundary layer can be easily created using both the cavity and shell functions of CAD, and IV: Simulated element for convection can be easily created using the cavity function of CAD. To perform highly accurate FEM thermal simulations, it is necessary to know the characteristic values of the four virtual models in advance.

5 Conclusion

(1) A method to calculate the temperature distribution due to fluid behavior in a structure was proposed by FEM thermal simulation using four virtual fluid elements; I: inflow, II: outflow, III: boundary layer, and IV: convection.

(2) In the steady-state analysis, the FEM thermal simulation using the proposed virtual fluid element was shorter than the FVM fluid simulation by about 4/9 to 1/285. The computational errors are 7/8 to 1/9 of those of the FVM fluid simulation, which is more accurate. For the unsteady state, the FEM thermal simulation with the proposed virtual fluid element takes about 2.1 to 3.1 times longer than the FVM fluid simulation. The computational errors are about 6/7 to 1/9 of those of the FVM fluid simulation.

References:

[1] A. Itou, T. Nakanishi, T. Saburi, S. Kubota, Y. Ogata, High Performance Parallel Computing for Computational Fluid Dynamics (CFD) -Second Report, *Komatsu technical report*, Vol.51, No.156, 2007, pp. 21-26 (in Japanese).

[2] J. Jedrzejewski, W. Modrzycki, Compensation of Thermal Displacement of High-speed Precision Machine Tools, *Journal of Mechanical Engineering*, Vol. 7, No. 1, 2007, pp. 108-114

[3] Z. Winiarski, Z. Kowal, J. Jedrzejewski, Precise Modelling of Machine Tool Drives with Ball Screw Thermal Behaviour, *Journal of Mechanical Engineerig*, Vol. 17, No. 1, 2017, pp. 31-45.

[4] RENESAS，“Mechanism of Heat radiation” https://www.renesas.com/jajp/support/technicalresources/package/characteristic/heat-01.html [Accessed on 25 February, 2023].

[5] J. Jedrzejewski, W. Kwasny, Z. Kowal, Z. Winiarski, Development of the Modelling and Numerical Simulation of Thermal Properties of Machine Tools”, *Journal of Machine Engineering*, Vol.14, No. 3, 2014, pp.5-20.

[6] J. Glanzel, T. S. Kumar, C. Nauman, M. Puntz, Parameterization of Environmental Influences by Automated Characteristic Diagrams for the Decoupled Fluid and Structural-machine Simulations”, *Journal of Machine Engineering*, Vol.19, No. 1, 2019, pp.98-113.

[7] Z. Lei, Y. Nagata, Development for a parallelized CFD code-ADCS, *JAXA Research and Development Report*, JAXA-RR-09-006, 2010, pp. 1-5.

[8] H. Sugiyama, M. Sano, Y. Nagahasi, N. Kato, Transfer Phenomenology to Learn for the First time - to Understand Momentum, Heat, Mass Transfer Integratedly – , *Morikita Publication*, 2014, pp. 110-155 (in Japanese).

Contribution of Individual Authors to the Creation of a Scientific Article (Ghostwriting Policy)

The authors equally contributed in the present research, at all stages from the formulation of the problem to the final findings and solution.

Sources of Funding for Research Presented in a Scientific Article or Scientific Article Itself

No funding was received for conducting this study.

Conflict of Interest

The authors have no conflicts of interest to declare that are relevant to the content of this article.